arXiv:1402.7315v1 [astro-ph.GA] 28 Feb 2014

Spiral Density Waves in M81. I. Stellar Spiral Density Waves

Chien-Chang Feng[1], Lien-Hsuan Lin[1], Hsiang-Hsu Wang[1] and Ronald E. Taam[1,2]

hhwang@asiaa.sinica.edu.tw

ABSTRACT

Aside from the grand-design stellar spirals appearing in the disk of M81, a pair of stellar spiral arms situated well inside the bright bulge of M81 has been recently discovered by Kendall et al. (2008). The seemingly unrelated pairs of spirals pose a challenge to the theory of spiral density waves. To address this problem, we have constructed a three component model for M81, including the contributions from a stellar disk, a bulge, and a dark matter halo subject to observational constraints. Given this basic state for M81, a modal approach is applied to search for the discrete unstable spiral modes that may provide an understanding for the existence of both spiral arms. It is found that the apparently separated inner and outer spirals can be interpreted as a single trailing spiral mode. In particular, these spirals share the same pattern speed 25.5 km s^{-1} kpc^{-1} with a corotation radius of 9.03 kpc. In addition to the good agreement between the calculated and the observed spiral pattern, the variation of the spiral amplitude can also be naturally reproduced.

Subject headings: spiral galaxies, spiral density wave, modal approach

1. Introduction

The magnificent spiral arms observed in disk galaxies have been proposed to be a quasi-stationary phenomenon of a wave since the mid-1960s (Lin & Shu 1964, 1966). The wave interpretation of spirals resolves the so-called winding dilemma problem that spirals would otherwise rapidly wrap up if a spiral is made of the same material in a differentially rotating disk. The stellar spiral arms are assumed to be a small perturbation superimposed on an

[1]Institute of Astronomy and Astrophysics, Academia Sinica, P.O. Box 23-141, Taipei 10617, Taiwan, R.O.C.

[2]Department of Physics and Astronomy, Northwestern University, 2131 Tech Drive, Evanston, IL 60208, USA

basic state and, therefore, can be understood with linear analysis. Within the framework of a density wave, the shape of spirals is determined by a dispersion relation, which is an intrinsic property of a self-gravitating disk. Soon in the late 1960s, the working hypothesis of quasi-stationary spiral structure (QSSS) led to the study of the non-linear gas response to the underlying stellar spirals. The bright new born stars along spirals are interpreted to be a result of gas compression as molecular clouds pass through galactic shocks (Roberts 1969). However, it was immediately recognized that the picture of the spiral density wave was not complete (Toomre 1969). The spiral structures are bound to disappear quickly as the wave packets propagate away from the disk. Hence, a feedback mechanism would be required to support the QSSS hypothesis.

In 1970s, both in hydrodynamics and stellar dynamics, a self-consistent theory of global spiral mode was developed to explain the excitation and maintenance of density waves. Unlike the early development of spiral density wave theory in which the pattern speed is determined empirically or inferred from observations, the modal approach associates the growth rates and the pattern speeds to the discrete eigenvalues that are subject to boundary conditions. The spiral patterns are identified as the corresponding eigen-functions of modes. In other words, spiral arms are considered to be the self-excited unstable modes with calculated pattern speeds and growth rates. The mechanisms of a wave amplification loop have been analytically explored in great detail by several authors (Mark 1976b, 1977; Lin & Lau 1979; Bertin et al. 1989; Bertin & Lin 1996; Bertin 2000).

Given various types of spiral galaxies, the above mentioned classical density wave theory, which views the grand design spirals as intrinsic unstable modes of disks, is by no means the only possibility for the self excitation of spirals. Spirals can be interpreted as collective responses to clumps in a density distribution (Goldreich & Lynden-Bell 1965; Julian & Toomre 1966; Toomre & Kalnajs 1991) and understood in terms of the so-called swing-amplification mechanism (Toomre 1981). For example, the global N-body simulations conducted by Sellwood (2012) show that the growth of non-axisymmetric waves can be characterized by two phases. The first, slowly growing phase is due to the swing-amplified shot noise that propagates inwards and is absorbed at the inner Lindblad resonance. The accumulating change in the distribution function at this resonance, owing to wave-particle interactions, leads to the second phase corresponding to the rapid growth of non-axisymmetric spirals. The exposure of the inner Lindblad resonance to incident wave trains is crucial for the operation of this mechanism. More recently, D'Onghia et al. (2013) demonstrate that apparent long-lived spirals can be a result of the non-linear development of gravitational wakes, which are initially induced by density clumps, such as giant molecular clouds. Once these wakes are formed, they may act as new perturbers to maintain the spiral forming activities. In this view, the grand design spirals are nothing more than connections between self-perpetuating wave seg-

ments so that the visually 'long-lived' structures are understood in a statistical sense. This mechanism may potentially play a role in forming spiral structures recently observed in red disk galaxies with no gas (Masters et al. 2010) and in dwarf elliptical galaxies in the Virgo cluster (Lisker et al. 2006; Lisker et al. 2009). Here, we do not attempt to complete the list of possible mechanisms as a more thorough discussion on this topic has been recently reviewed by Sellwood (2013). However, we believe that different theories or mechanisms may operate in different types of spiral galaxies during secular evolution. Distinguishing between different possibilities for a specific galaxy can only rely on qualitative and quantitative comparisons between theoretical predictions and observations. In the following, we apply the modal analysis to the galaxy M81 within the framework of spiral density wave theory to confront the observations.

M81 (NGC 3031) is one of the most well-studied spiral galaxies due to its proximity to the Milky Way and its good inclination, which is suitable for extracting kinematic information. The presence of a central bright bulge together with the nearly bi-symmetric spiral arms found in the galactic disk make M81 one of the best targets for investigating the origin of spiral structure. Visser (1980b) applied the dispersion relation to a basic model for M81 to fit the shape of stellar density wave observed outside the radius of 3.5 kpc. The pattern speed, $\Omega_p = 18$ km s^{-1} kpc^{-1}, was chosen based on the morphology of spirals and also artificially constrained by the computational consideration for the non-linear gas response discussed in the second paper (Visser 1980a). In this particular model, density wave theory failed to explain structures situated inside the inner Lindblad resonance (ILR), which is located at 2.5 kpc.

Lowe et al. (1994) revisited the problem of spiral density waves in M81 based on the modal approach. A set of formulae was proposed to fit the observed rotation curve and the mass distribution of the disk in the range of $4 < r < 15$ kpc. The authors interpreted the variation of the spiral amplitude observed in the *I*-band image (Elmegreen et al. 1989) as a result of the interference of trailing and leading waves that are propagating in the opposite directions. In their best-fit model, the pattern speed is determined to be $\Omega_p = 24$ km s^{-1} kpc^{-1} with the corresponding corotation radius located at 9 kpc. The pattern speed is in good agreement with value, $\Omega_p = 26$ km s^{-1} kpc^{-1}, determined by the non-linear response of gas at the 4:1 resonance (Elmegreen et al. 1989) as well as with the value, $\Omega_p = 23.4 \pm 2.3$ km s^{-1} kpc^{-1}, obtained by integration of the continuity equation (Tremaine & Weinberg 1984; Westpfahl 1998). However, the presence of the inner turning point at 4 kpc again rules out the possibility of wave propagation in the central region $r < 4$ kpc. As also cautioned in Lowe et al. (1994), their analysis might be biased by the lack of reliable data in the red and infrared wavelengths at that time.

Recently, Kendall et al. (2008) used *Spitzer* IRAC 3.6 and 4.5 μm near-infrared data from the Spitzer Infrared Nearby Galaxies Survey(SINGS), optical B, V and I and Two-Micron All-Sky Survey K_s-band data to trace the spiral density waves in M81. Using the data of different wavelengths enabled the authors to produce maps of stellar mass surface density and remove possible contaminations arising from young stars and from polycyclic aromatic hydrocarbons (PAHs). The non-axisymmetric structures (residuals) are then extracted by subtracting the axisymmetric component from the original maps. As the residual map of IRAC 3.6 μm shown in Fig. 1, aside from the outer stellar spirals, which are usually the primary focus in previous studies of M81, another pair of stellar spirals is revealed well inside the bright bulge of M81. As already noted in Kendall et al. (2008), both models as discussed in Visser (1980b) and Lowe et al. (1994) fail to explain the presence of the inner stellar spirals. In these theoretical investigations, the bulge region is considered dynamically hot and is, therefore, hostile to the presence of density waves.

Furthermore, as also shown in Kendall et al. (2008), a good correlation is found between the inner dust spirals (IRAC 8 μm) and the inner stellar spirals (IRAC 3.6 μm). Since within the framework of density wave theory where density waves in the gas are allowed to propagate through the inner Lindblad resonance, Kendall et al. (2008) interpreted the stellar spirals as a result induced by the gas spirals. However, from the dynamical point of view, it is unlikely that the inner stellar spirals can be induced by the gas spirals for the following reasons. First, the velocity dispersion in stars is much larger than that of gas in the bulge region. If we adopt the values from Lowe et al. (1994), the radial velocity dispersion in stars can be easily more than 40 km s^{-1} (cf. for the central region of the Milky Way) in the central region in contrast to the value $\approx$ 10 km s^{-1} for the gas. Since the energy involved is proportional to the square of velocity dispersion, transferring energy from the gas to stars is not effective in perturbing the stellar system. Second, little amount of gas is found in the bulge compared to the stellar mass. The total mass of the widespread HI in M81 is estimated to be 2.6×10^9 M$_\odot$ (Yun et al. 1994) in contrast to the more concentrated bulge mass enclosed within 3 kpc of 1×10^{10} M$_\odot$ (Lowe et al. 1994). Third, the thickness of the gas disk is much thinner than that of the stellar disk. In other words, the density waves in gas only effectively influence stars that are close to the mid-plane. Fourth, the absence of an ILR as shown in Westpfahl & Adler (1996) does not support the possibility of wave excitation in gas at the radius of resonance. The non-linear gas response is basically forced by the underlying stellar spirals and belongs to the type of waves discussed in Roberts (1969) (see also Fujimoto (1966); Shu et al. (1973); Woodward (1975)).

The models proposed by Lowe et al. (1994) and Visser (1980b) are not compatible to the presence of the newly discovered inner spiral structure. With little details regarding the inner stellar spirals given in the literature, the origin and the property of the inner stellar

spirals is elusive. Despite these difficulties, the faint tails of the inner spirals as shown in Fig. 1 hint that the inner and outer spirals may be a single spiral mode. The seemingly separate structure is simply due to low density contrast if one compares the amplitude of the spirals to the bright axi-symmetric background. If this is a plausible interpretation, the following can be inferred. First, the inner and outer arms share the same pattern speed, which has been more or less constrained in the literature for the outer spirals. Second, from a dynamical consideration, the ILR may be absent as discussed in Adler & Westpfahl (1996), and the turning point has to be placed roughly at $r = 1.4$ kpc. The location of the turning point as so chosen in Lowe et al. (1994) is somewhat driven by the requirement of wave behavior, i.e., the wave is not allowed to propagate in the region of $r < 4$ kpc. In general, the presence of a turning point is not guaranteed for a given rotation curve. Third, the coincidence of gas(dust) and stellar spirals is a natural outcome of the theory of spiral density waves. The non-linear gas response to the underlying stellar potential is an active subject in the field.

Unlike the work of Lowe et al. (1994), who use heuristic formulae to fit the rotation curve of M81 for the range $r > 4$ kpc, we start with a three-component model associated with a bulge, a dark halo, and an active stellar disk. The mass model is constructed to fit the whole range of the observed rotation curve and to fit the observed mass distribution. The resultant rotation curve is then treated as input for the modal analysis. With this procedure and proper boundary conditions, we obtain unstable spiral modes that may explain the existence of spirals observed in M81. This paper is structured as follows. The three component model and the procedure of modal analysis are detailed in §2. In §3, we present the results obtained from the modal analysis and its comparison with observational data. The results are discussed in §4 and we summarize in the last section.

2. Method of Analysis

2.1. Observational Constraints and A Three-component Model for M81

We apply the modal approach described in Lau & Bertin (1978) to a zero-thickness fluid disk model for M81 to search for discrete global unstable modes that may account for the seemingly separated inner and outer spirals. The prominent bright bulge of M81 and the presence of inner spirals suggest that the central region is probably composed of a dynamically hot bulge and a relatively cold disk, within which the density wave can propagate. It is also well established that the rotation in the outer region of a disk galaxy is usually dynamically supported by a dark halo. Thus, the basic state of M81 is taken to be composed of an active stellar disk and two inactive spherical components, a bulge and a dark matter halo,

which are usually dynamically hot and not involved in the propagation of spiral waves. The well-observed rotation curve is therefore associated with a three-component model composed of a stellar disk, a bulge, and a dark halo.

The formula used to describe the density distribution of the spherical halo is given by (Lowe et al. 1994):

$$\rho_{\rm H}(R) = \frac{\rho_{\rm H0}}{1 + (R/R_{\rm H})^2}, \tag{1}$$

with $\rho_{H0} = 3.5 \times 10^7$ M$_\odot$ kpc^{-3} corresponding to the central volume density, R the distance and $R_{\rm H} = 2.8$ kpc a length scale controlling the concentration of the halo. The total mass $M_{\rm H}$ enclosed within the radius of 12 kpc is 2.84×10^{10}M$_\odot$. For the model of the bulge, we adopt the form described in Athanassoula (1992),

$$\rho_{\rm b}(R) = \rho_{\rm b0} \left(1 + \frac{R^2}{R_{\rm b}^2}\right)^{-1.5} \tag{2}$$

with $\rho_{\rm b0} = 5.5 \times 10^8$ M$_\odot$ kpc^{-3} corresponding to the central volume density and $R_{\rm b} = 1$ kpc, the concentration factor of the bulge. The total mass of the bulge enclosed within the radius of 12 kpc is $M_{\rm b} = 1.5 \times 10^{10}M_\odot$. As for the surface density of the active stellar disk, we adopt the combination of two Toomre's disks (Toomre 1963; Lau & Bertin 1978),

$$\sigma_0(r) = \frac{4.5 M_1}{\pi a_1^2} \frac{1}{x_1^{11}} - \frac{4.5 M_2}{\pi a_2^2} \frac{1}{x_2^{11}} \tag{3}$$

with $M_1 = 6.9 \times 10^{10}$ M$_\odot$, $M_2 = 7 \times 10^9$ M$_\odot$, $a_1 = 10$ kpc, $a_2 = 7$ kpc, $x_j = [1 + (r/a_j)^2]^{1/2}$, $j = 1, 2$, and r the radial distance measured in the disk plane. The mass in the active stellar disk, $M_{\rm d}$, is 6.2×10^{10}M$_\odot$. The scale length of the active disk fitted to an exponential profile for the range between 3 kpc and 10 kpc is estimated to be 2.5 kpc. This value is in excellent agreement with the observational value of 2.5 kpc (Kent 1987) and is consistent with the value 2.83 kpc adopted in Lowe et al. (1994). Comparisons of our mass model with other works are summarized in Table 1.

Figure 2 shows the observed rotation curve as well as the fitting curve using the three-component model and the above parameters. The observed rotational velocity in the outer disk is traced using neutral hydrogen (Adler & Westpfahl 1996; Kent 1987), while for the inner disk a few data points from the CO observation are adopted (Sage & Westpfahl 1991). In this plot, all the observational data points have been normalized for the distance of M81 adopted in Kendall et al. (2008), i.e., 3.6 Mpc. The contributions from the disk, the bulge and the dark halo are presented in dashed, dash-dotted and dotted lines, respectively. The fitting rotation curve, shown as the solid line, is in good agreement with the observational data. The reason of choosing these models is to ensure the central part of the M81 behaves

as a solid body rotating with nearly the same angular speed. This feature is important for circumventing the singularity that would otherwise occur in the modal analysis (details described below). We avoid the use of popular models for the shape of the dark matter halo such as NFW (Navarro et al. 1997) or Hernquist (Hernquist 1990) profiles for the following reasons. First, both of them have a density cusp at the center of galaxies which is not directly supported by observations. On the contrary, a constant dark matter density seems to be preferred in the inner parts of galaxies (de Blok 2010) and is, therefore, well described by Eq. (1). Secondly, and more important, is that both profiles leads to infinite angular speed as the galactic center is approached, which is physically unrealistic.

Aside from the active surface density, $\sigma_0(r)$, and the angular speed, $\Omega(r)$, which can be derived from the rotation curve, another constraint associated the basic state is the radial profile of the sound speed, $a(r)$, defined within the framework of fluid description. Our knowledge about $a(r)$ is very limited and can only be inferred from an understanding of the stellar dynamics. The sound speed is related to Toomre's Q through the following relation:

$$Q(r) = \frac{a\kappa}{\pi G\sigma_0}, \tag{4}$$

where G is the gravitational constant and κ is the epicyclic frequency. The Q profile provides a description of the stability and hotness of the disk. For a zero-thickness disk, $Q < 1$ indicates that the disk is unstable with respect to axisymmetric perturbations. The disk would quickly evolve and settle down to a new basic state, making the description for the original basic state inconsisten. On the other hand, $Q \gg 1$ suggests that the disk is dynamically hot and stable. Structures developed in such a disk would not survive sufficiently long to account for the frequency of grand-design spiral galaxies. Following these dynamical considerations, one can conclude that $Q(r)$ should be greater than but not far from unity. We, therefore, adopt the following description for Q:

$$Q = \alpha_0 + \Sigma_{i=1}^{3}\alpha_i \exp[-(r-\beta_i)^2/\gamma_i^2], \tag{5}$$

with $\alpha_0 = 1.0$ and $(\alpha_i, \beta_i, \gamma_i)$ summarized in Table 2. The Q profile is composed of a constant term and three Gaussian functions. The coefficients, $\alpha_1, \beta_1, \gamma_1$, describe a disk which is stable to the axisymmetric perturbation, while the coefficients, $\alpha_2, \beta_2, \gamma_2$ result in the steep rising Q, reflecting the fact that the active disk in the bulge region is dynamically hot as compared to the outer disk. The negative contribution from the set, $\alpha_3, \beta_3, \gamma_3$, is added to adjust the behavior of k_3^2 near corotation in order to achieve appropriate growth rates, pattern speeds, spiral patterns and spiral amplitudes. This indicates that the behavior of Q near corotation is critical to the wave amplification. The resultant Q profile and the corresponding sound speed are shown in Fig 3. The sound speed roughly flattens at 76 km s^{-1} in the bulge region. The corresponding values at corotation and the outer 4:1 resonance are 18.0 and 9.0 km s^{-1},

respectively. Due to the lack of a direct measurement of the radial velocity dispersion of M81, in the process of modelling, the Q profile can be only roughly constrained by the wave phenomenon as seen in the image Fig. 1 and guided by the theory of spiral density wave described below.

2.2. Modal analysis

Following Lau & Bertin (1978), the hydrodynamic equations are formulated in cylindrical coordinates, (r, ϕ, z), with its origin placed at the galactic center. We consider a density perturbation σ_1 and all associated perturbed quantities are proportional to $\exp[i(\omega t - m\phi + \int^r k dr)]$, with m corresponding to the number of spirals and k the radial wave number. Using this representation, negative k traces trailing spirals. Treating $\epsilon = a/\kappa r$ as a small parameter, the Poisson equation (Bertin & Mark 1979) together with the hydrodynamical equations can be systematically expanded to include terms of order ϵ^2. We note that this is an excellent approximation for most of the region of our interest except for the very inner part ($\epsilon > 1$ for $r < 0.3$ kpc) of the model, where the amplitude of wave is small due to the evanescent nature of the wave. Nevertheless, direct comparisons between the results obtained from exact calculations, i.e., solving a set of integro-differential equations, and from asymptotic approximation have been shown to be in a good agreement (Pannatoni & Lau 1979). For simplicity, we therefore assume that the governing equation based on small ϵ^2 is applicable throughout the region including the galactic center. Consequently, the equation we solved for discrete spiral modes is the following differential equation for the enthalpy perturbation $h_1 = a^2\sigma_1/\sigma_0$ (see the Appendix B in Lau & Bertin (1978) for the details of derivation),

$$\frac{\mathrm{d}^2 u}{dr^2} + k_3^2 u = 0, \tag{6}$$

where

$$h_1 = u\left[\frac{\kappa^2(1-\nu^2)}{\sigma_0 r}\right]^{1/2} \exp\left(-i\int^r \frac{\kappa}{aQ} dr\right), \tag{7}$$

$$k_3^2 = \hat{k}_3^2 + k_{\rm co}^2 + k_{\rm img}^2 + k_{R_1}^2 + k_{R_2}^2. \tag{8}$$

Here, $\nu = (\omega - m\Omega)/\kappa$ is the Doppler-shifted frequency and u is an auxiliary function under the transformation Eq. (7). The first term on the right of Eq. (8), which is the major term discussed in Lau & Bertin (1978) is given by

$$\hat{k}_3^2 = \left[\frac{\kappa}{a}\right]^2 \left[\frac{1}{Q^2} - 1 + \nu^2 + \frac{1}{4}\mathscr{J}^2 Q^2\right], \tag{9}$$

$$\mathscr{J} = 2m\left(\frac{\pi G\sigma_0}{\kappa^2 r}\right)\left(\frac{1}{s}-\frac{1}{2}\right)^{-1/2}, \tag{10}$$

$$s = -d\ln\Omega/d\ln r. \tag{11}$$

In addition to $\hat{k}_3^2$, we also consider the term associated with the corotation resonance $k_{\rm co}^2$, the "out of phase" term $k_{\rm img}^2$ and the two remaining terms $k_{R_1}^2$ and $k_{R_2}^2$ defined as follows:

$$k_{\rm co}^2 = -\frac{2\Omega m}{\kappa\nu r^2}\frac{d\ln(\kappa^2/\sigma_0\Omega)}{d\ln r}, \tag{12}$$

$$k_{\rm img}^2 = -\frac{i\Sigma}{2}\frac{d}{dr}\ln[Q^2(1-\nu^2)], \tag{13}$$

$$k_{R_1}^2 = \frac{3}{4r^2} - \left[\frac{r\kappa^2(1-\nu^2)}{\sigma_0}\right]^{1/2}\frac{d^2}{dr^2}\left[\frac{\sigma_0}{r\kappa^2(1-\nu^2))}\right]^{1/2}, \tag{14}$$

$$k_{R_2}^2 = -\frac{4m(\Omega/\kappa)\nu[m\nu r(\Omega'/\kappa)+r\kappa'/\kappa]}{r^2(1-\nu^2)}. \tag{15}$$

In Eq. (12), we have replaced the singular factor $1/\nu$ by the "plasma dispersion relation", $-b\bar{Z}(b\nu)$, when approaching the corotation radius to take into account the smoothing effect associated with the epicyclic motions of stars (Mark 1976a,b; Lau & Bertin 1978; Lau 1994) where

$$\bar{Z}(\zeta) = -2i\exp(-\zeta^2)\int_{-\infty}^{-i\zeta}\exp(-t^2)dt, \tag{16}$$

and the factor b is defined by:

$$b = \frac{1}{\sqrt{2}r_{\rm co}\epsilon\nu'}. \tag{17}$$

Here, $r_{\rm co}$ is corotation radius and ν' the derivative of ν with respect to r. The connection between $1/\nu$ and $-b\bar{Z}(b\nu)$ is rather smooth as in the limit $\epsilon \to 0$, $-b\bar{Z}(b\nu) \to 1/\nu$. The eigenvalue $\omega = \omega_r + i\omega_i$ of the second-order differential equation Eq. (6) is now determined by imposing the following boundary conditions:

$$\frac{du}{dr} = 0 \qquad \text{at} \qquad r = 0, \tag{18}$$

$$\frac{1}{u}\frac{du}{dr} = -ik_3 - \frac{1}{2}\frac{d\ln k_3}{dr} \qquad \text{at} \qquad \nu_r = (\omega_r - m\Omega)/\kappa = 0.5. \tag{19}$$

The first condition assumes that the center of the galaxy is a node of the wave, while the second condition is a radiation condition, reflecting the absorption of short trailing wave at the outer Lindblad resonance where ν_r=1. This choice automatically rules out the possibility of considering any signal from the outer physical boundary and implicitly favors trailing

waves. Ignoring the possibility of leading waves should not be restrictive for the purpose of this work, i.e., to provide a dynamical explanation for the grand-design trailing spirals in M81. The leading waves are considered to play a minor role in modulating the amplitude of the spirals. Since the fluid description of spiral density waves is only appropriate within the principal region defined by $|\nu_r| < 1$, the choice of the inner and outer boundaries should be sufficiently far from the radii of the Lindblad resonances ($|\nu_r| = 1$). As a consistency check, there is no ILR associated with our model. Placing the outer boundary at the radius of the outer 4:1 resonance is also a reasonable choice for the fluid description.

In principle, one may obtain solutions by integrating the differential equation Eq. (6) using standard numerical methods if k_3^2 is a smooth function over the calculation domain. However, as $r \to 0$, the behavior of the terms $\mathscr{J}$, $k_{R_1}^2$ and $k_{R_2}^2$ depends on the behavior of the rotation curve. In general, a singularity would appear at $r = 0$, making direct integration numerically difficult. To circumvent this problem, either a proper inner boundary condition is imposed at a radius away from $r = 0$ or the behavior of the rotation curve can remove the singularity. For the later possibility, it is straightforward to show that solid body rotation, as modelled in Sec. 2.1, leads to all these terms converging to a finite value at $r = 0$.

3. Results

Given a basic state as described in Sec. 2.1, the governing equation (6) together with the boundary conditions Eqs. (18)(19), the eigenvalues, ω, and the corresponding eigenfunctions of the system can be found by numerical integration. In general, ω is complex in order to match both the real and imaginary parts at the boundaries. Under the assumption of a quasi-stationary spiral structure (QSSS), the pattern speed, Ω_p, is associated with the real part through, $\omega_r = m\Omega_p$, while the imaginary part is identified as the temporal growth rate of the spiral mode. Unlike the work of Visser (1980b), where the pattern speed, $\Omega_p = 18$ km s^{-1} kpc^{-1}, is constrained by the shape of outer spirals and by some computational considerations, within the framework of modal analysis, the pattern speed in this work is determined by the theory and, therefore, is consistent with the reaction of the given basic state. In other words, the basic state constructed from a real galaxy must be in a configuration such that a proper response and pattern speed is obtained as observed.

The solutions of Eq. (6) can be classified according to the terms of (m, n), where m is the number of spiral arms and n represents the number of nodes. As the residual map shown in Fig. 1 has nearly bi-symmetric inner and outer spiral arms, we seek eigenvalues and eigenfunctions of $m = 2$ for the three-component model. For the mode $n = 0$, we find $(\omega_r, \omega_i) = (69.0, -4.8)$, while for $n = 1$, $(\omega_r, \omega_i) = (51.0, -4.5)$. These eigenvalues are

insensitive to the inner boundary condition if Eq. (18) is replaced by $u = 0$ and to the exact location of the outer boundary if it is shifted slightly from the 4:1 resonance. The negative ω_i indicates that these modes are unstable and therefore their amplitudes are exponentially growing with time. Direct comparisons between the calculated and the observed data such as the pattern speed, the spiral pattern as well as the spiral amplitude lead us to conclude that the apparent separate inner and outer spiral arms can be explained by a single mode $(m = 2, n = 1)$. The reason that the mode $(m = 2, n = 1)$ dominates over the mode $(m = 2, n = 0)$ can be understood as a result of tidal interaction with the companions M82 and NGC 3077 between 200 to 400 Myrs ago (Thomasson & Donner 1993; Yun 1992; Yun et al. 1993). Since the growth rate of these two modes are comparable, the interaction provided a perturbation that favors the mode $(m = 2, n = 1)$.

The pattern speed of this mode is found to be $\Omega_p = 25.5$ km s^{-1} kpc^{-1}. The corresponding radii of corotation and outer 4:1 resonance are located at 9.0 kpc and 10.8 kpc, respectively. Compared with the typical pattern speeds quoted in the literature, our value is significantly higher than those that are more or less around 18 km s^{-1} kpc^{-1} (Shu et al. 1971; Rots 1975; Visser 1980a,b; Gottesman & Weliachew 1975; Sakhibov & Smirnov 1987; Kendall et al. 2008). However, our result is in good agreement with those estimated around 25 km s^{-1} kpc^{-1} (Roberts et al. 1975; Elmegreen et al. 1989; Lowe et al. 1994; Westpfahl 1998). The location of the corotation in our model is also consistent with the values around 9 kpc quoted in the latter references mentioned above.

The radius of the outer 4:1 resonance defines the outer boundary of our calculation. We note the absence of an inner Lindblad resonance associated with this pattern speed. Upon substituting this eigenvalue into Eq. (8), the curves of k_3^2, $\hat{k}_3^2$ as well as the sum of remaining terms are shown in Fig. 4. The real and imaginary parts associated with these quantities are presented separately in black and red. From this figure, we first note that in the central region ($r < 2$ kpc), both $\hat{k}_3^2$ and the remaining terms $(k_3^2 - \hat{k}_3^2 = k_{\rm co}^2 + k_{\rm img}^2 + k_{R_1}^2 + k_{R_2}^2)$ contribute to the behavior of the wave. While the term $\mathbf{Re}(\hat{k}_3^2)$ is positive as the center is approached, the negative contribution making the $\mathbf{Re}(k_3^2)$ less than zero is primarily from $\mathbf{Re}(k_{R_2}^2)$ and $\mathbf{Re}(k_{\rm co}^2)$. On the other hand, the imaginary part, $\mathbf{Im}(k_3^2)$, peaked around $r = 0.6$ kpc is mainly from the term $\mathbf{Im}(k_{\rm imag}^2)$. As can be seen, all the terms on the right of Eq. (8) play a role in the analysis.

From Fig. 4, it is important to realize that the imaginary part of k_3^2 should not be neglected in this model. The condition that one can ignore the imaginary part is that the Q-barrier, where $\mathbf{Re}(k_3^2) = 0$, is sufficiently far away from the region where $\mathbf{Im}(k_3^2)$ is significant. This is usually attributable to the fact that the density wave exponentially decays inside the Q-barrier, where $\mathbf{Re}(k_3^2) < 0$, before the term $\mathbf{Im}(k_3^2)$ takes effect. However, this condition

does not apply to our model since the 'turning point' is located near the peak of $\mathbf{Im}(k_3^2)$. As a result, the real and imaginary parts of u are no longer in phase. The concept of Q-barrier defined by the tuning point in $\mathbf{Re}(k_3^2)$ is not useful in this particular model. Nevertheless, the auxiliary function u is forced to decay to zero in our model because of the boundary condition imposed at $r = 0$.

For a given k_3^2 and the boundary conditions, $u = u_r + iu_i$ can be determined through numerical integration. Here, (u_r, u_i) are the real and imaginary parts of the auxiliary function $u(r)$, respectively. The perturbed enthalpy h_1 and the corresponding perturbed surface density, σ_1, can be calculated through the transformation Eq. (7) and the relation $\sigma_1 = h_1\sigma_0/a^2$. In Fig. 5, we overlap the contours of the calculated density wave for the specific mode $(m = 2, n = 1)$ on the residual image of 3.6 μm. The good agreement between the observation and the theoretical calculation suggests that the inner spirals together with the outer spirals can be explained by the presence of a single spiral mode. In particular, they share the same pattern speed 25.5 km s^{-1} kpc^{-1}. The fact that the seemingly separated inner and outer spirals belong to the same spiral mode is more clearly seen in Fig. 1.

In Fig. 6, the relative amplitude obtained from the mode analysis is rescaled to fit the observed IRAC 3.6, 4.5 μm and I-band data as shown in Kendall et al. (2008). Here, the relative amplitude is defined as $\sigma_1/(\sigma_0 + \sigma_{\rm b})$, which is consistent with the definition adopted in Kendall et al. (2008). We note that when calculating the relative amplitude, the projected mass of bulge, $\sigma_{\rm b}$, is taken into account since both the disk and the bulge contribute to the axisymmetric part of luminosity. The grey dash-dotted lines bracket the uncertainty of the amplitude of IRAC 3.6 μm. There is no observed information regarding the relative amplitude of the inner spirals. The calculated result (solid curve) is shown for the range inside the radius of outer 4:1 resonance, which is the domain of calculation. The general trend shows that the observed relative amplitude is rising with increasing radius and starts to drop off roughly between 9 to 11 kpc depending on the observed wavelength. It is evident that within the range of uncertainty the general trend of the calculated amplitude (solid curve) fits the observation reasonably well. The low density contrast in the central region ($r < 3.5$ kpc) can explain the lack of a detected spiral embedded in the bright bulge. The small variations superimposed on the observed amplitude may be interpreted as the interference pattern of leading and trailing modes as discussed in Lowe et al. (1994), which is beyond the scope of this paper.

4. Discussion

In this work, we interpret the stellar response of a mass model for M81 as an unstable spiral mode in a zero-thickness fluid disk. The component that actually participates in the wave propagation is the active stellar disk. The bulge and the dark matter halo components are treated as static structures to support the observed rotation curve. Lowe et al. (1994) introduce a mass reduction factor f for an exponential disk to incorporate the effect of gravity dilution due to the disk thickness. Their active disk density profile is therefore given independently of the rotation curve. Despite the fact that the factor f originates from the dynamical consideration, we have not introduced this additional adjustable function in modeling the non axisymmetric structure for two reasons. First, it is well-known that decomposing the surface light profile into different mass components is somewhat ambiguous especially for the bulge region, since the formation process of bulges (or pseudo-bulges) and the origin of exponential disks remain unclear. Second, a degeneracy exists in using parameters for three-dimensional models in fitting observed two-dimensional data. Thus, we simply adopt $f = 1$ to minimize the degrees of freedom in the modelling process. In fact, the coefficients $(\alpha_1, \beta_1, \gamma_1)$ that lead to departures of the Q-profile from unity implicitly include information of the disk thickness.

Since M81 is not a gas-rich galaxy, we have neglected the limited impact of gas on the stellar dynamics in our analysis. However, the dissipative gas may play important roles in maintaining stellar density waves. In addition to facilitating the formation of new stars through shock compression (Roberts 1969), the interstellar medium also serves as a coolant that saturates the amplitude of the growing stellar spiral and sustains the conditions for the occurrence of grand-design spirals for a relatively long time (Roberts & Shu 1972; Bertin et al. 1989; Contopoulos & Grosbol 1986; Patsis et al. 1994). Furthermore, since the density waves in the gas can be transmitted beyond the outer Lindblad resonance, the conservation of wave action may lead to the spirals in atomic gas that lie well beyond the optical disk (Bertin & Amorisco 2010). The incompleteness of our model is related to the relatively low sound speed calculated for the outer 4:1 resonance, where the surface density of gas may be significant to raise the sound speed to the level required for it to be gravitationally stable. Since the equations in our study do not include the dissipative nature of gas as well as the interaction between gas and stars, we leave the sound speed as assumed.

The radius of corotation of the spiral pattern in M81 has been determined through various methods as summarized in the Section 5.2 of Kendall et al. (2008). We do not repeat them here, but comment on the method used by Kendall et al. (2008), which is based on the phase offset between the stellar spiral and 8-μm emission. It is known from asymptotic analyses as well as from numerical simulations that there exists a angular shift between the peak

of the gas shock and the potential minimum of the stellar arm (Roberts 1969; Visser 1980a; Gittins & Clarke 2004). Here, we have implicitly assumed that the dust emission at 8-μm traces the shock locations. Gittins & Clarke (2004) performed hydrodynamical simulations without self gravity to systematically study the non-linear gas response to imposed rigidly rotating stellar spirals. Inside corotation, the gaseous shocks are offset in the upstream direction with respect to the potential minimum. Although the actual shift depends on the strength of the spirals and the sound speed of the gas, the general trend is that the phase offset increases as the corotation radius is approached. Based on the simulation results, they conclude that for two-armed spirals the radius of corotation can be determined to within 25 per cent if the angular offset exceeds $\approx \pi/4$. However, the active star formation as observed along spirals suggests that the self gravity of gas is important to the gasdynamics around shocks and therefore may significantly affect the phase shift. The influence of self gravity on the determination of corotation radius based on the phase-offset method will be discussed in a subsequent paper.

'Halo-disk degeneracy' is an outstanding issue when decomposing an observed rotation curve into a luminous disk and a dark matter halo (Bershady et al. 2010). This is largely due to the uncertainty in the mass-to-light ratio and its radial dependence, which depends on the models of star formation history as well as of the initial mass function. Furthermore, even for luminous components, the bulge-disk decomposition introduces a further uncertainty when modelling the mass distribution of M81. The presence of inner spirals inside the bulge suggests the co-existence of disk and bulge in the central region. Despite these difficulties, Eq. (6) associates a proper disk response to a proper surface mass of an 'active' disk, which might be considered as the lower limit of the disk mass or mass-to-light ratio. As shown in Table 1, the total luminous mass of our model is about 88% of the maximum-disk mass, which is estimated to be 8.7×10^{10} $M_\odot$ (Kent 1987). In order to have the correct stellar disk response, it is interesting to note that the mass decomposition of our model is quite similar to that of Lowe et al. (1994) and Kent (1987). An additional diagnostic of the mass model may be obtained from the study of the non-linear gas response to the observed stellar spiral. Given the observed spiral strength and the distribution of gas, the reaction of self-gravitating gas should be compared to the substructures as seen in IRAC-8μm image. We will show in the second paper that only the proper strength of spirals, which is associated with a proper disk model, can have an appropriate gas response.

The absence of inner Lindblad resonance associated with the pattern speeds as reported in this work and inferred from recent observations seems to rule out the spiral-generating mechanism proposed by Sellwood (2012). There is, however, a possibility that the inner spirals in M81 rotate at a pattern speed different from that of the outer spirals. In this case, the pattern speed of the inner spirals should be lower than 25.5 km s^{-1} kpc^{-1}. It is also

possible that the inner and outer spirals are simply self-perpetuating spiral features as a result of the non-linear development of gravitational wakes (D'Onghia et al. 2013). As these two sets of spirals are virtually separated at the current epoch, it is not immediately clear what these possibilities imply for the future evolution of M81. In fact, for this particular case M81, the appearance of inner spirals in the nearly uniform rotating part of the disk also poses a challenge for the picture of swing amplification in the first place, since the important ingredients for this mechanism such as shear and epicyclic motions are no longer coherent in this region. Nevertheless, we emphasize that more than one mechanism may operate for spiral galaxies that are in different evolutionary states or environments.

Although this work is based on several assumptions on the model, three predictions obtained from this particular work can be checked observationally. First, the pattern speed of the inner spirals is the same as the outer spirals. Second, the velocity dispersion as a function of galactocentric distance is constrained by the shape and the strength of spirals. Third, the strength of inner spirals as shown in Fig. 6 requires observational confirmation.

5. Summary

The recent discovery of inner stellar spirals lying well inside the bright bulge of M81 cannot be understood within the framework of the models proposed by Visser (1980b) and Lowe et al. (1994) based on the theory of spiral density waves. With little information on the inner spirals in the literature, Kendall et al. (2008) interpreted that the inner stellar arms are probably induced by the density waves in gas. However, from the dynamical point of view, it is unlikely that the gas in the bulge region can effectively affect the wave behavior of stars. Hints from the image as shown in Fig. 1 and by the good correlation between dust spirals and stellar spirals suggests that the inner spirals together with the grand-design outer spirals may belong to the same spiral mode.

As the first step, a three-component model associated with an active stellar disk, a bulge and a dark matter halo is constructed to fit the observed rotation curve and the observed mass distribution. The resultant rotation curve is treated as an input function for the mode analysis. Given the boundary conditions, we follow the procedure described in Lau & Bertin (1978) and solve for the discrete eigenvalues and the corresponding eigenfunctions. In this description, the eigenvalues are associated with pattern speeds and growth rates of the modes and the eigenfunctions are related to the spiral patterns. Two dominant unstable modes with comparable growth rates were found for $m = 2$ in our calculations. The mode $(m = 2, n = 1)$ alone can explain most of the observed characteristics of the stellar spirals in M81. Specifically, the pattern speed is determined to be $\Omega_p = 25.5$ km s^{-1} kpc^{-1} and the

corresponding radius of corotation is located at 9 kpc. By directly overlapping the calculated density contours on the observation image as shown in Fig. 5, the apparent unrelated inner and outer spirals can be identified as the same spiral mode, rotating rigidly with the same pattern speed. Furthermore, the trend of the observed relative amplitude of the spiral can be well reproduced also from the mode analysis. This particular mode is likely 'selected' by the three-way interaction with M82 and NGC 3077 in the not too distant past.

Although the results obtained from this work qualitatively and quantitatively reproduce the observational data well, some ingredients associated with a disk galaxy were not taken into account in the mode analysis. For example, the effects of the disk thickness and of the interstellar medium are neglected as a first approximation. The latter neglect is dynamically important to the outer disk where the surface density of the gas disk is comparable to that of the stellar disk. Also the dissipative nature of the gas may be responsible for sustaining and regulating the amplitude of stellar spirals. It would be desirable to have measurements of the sound speed (radial velocity dispersion) as a function of radius in as much that it enters into the form of the Toomre Q parameter. The advent of Integral-Field-Unit (IFU) spectroscopy with two-dimensional coverage on the sky has provided the possibility of measuring the stellar velocity ellipsoid over galactic disks (Bershady et al. 2010). In a subsequent paper, the non-linear gas response to the underlying stellar potential obtained from this work will be discussed in detail.

The authors would like to acknowledge the support of the Theoretical Institute for Advanced Research in Astrophysics (TIARA) based in Academia Sinica Institute of Astronomy and Astrophysics (ASIAA). We are grateful to G. Bertin, Y. Y. Lau and F. Shu for the valuable inputs and discussions. The authors thank the referee for comments which helped to improve the clarity and presentation of this paper. Thanks to Mr. Sam Tseng for assistance on the computational facilities and resources (TIARA cluster).

REFERENCES

Adler, D. S., & Westpfahl, D. J. 1996, AJ, 111, 735

Athanassoula, E. 1992, MNRAS, 259, 328

Bershady, M. A., Verheijen, M. A. W., Swaters, R. A., et al. 2010, ApJ, 716, 198

Bertin, G. 2000, Dynamics of Galaxies

Bertin, G., & Amorisco, N. C. 2010, A&A, 512, A17

Bertin, G., & Lin, C. C. 1996, Spiral structure in galaxies a density wave theory

Bertin, G., Lin, C. C., Lowe, S. A., & Thurstans, R. P. 1989, ApJ, 338, 78

Bertin, G., & Mark, J. W.-K. 1979, SJAM, 36, 407

Contopoulos, G., & Grosbol, P. 1986, A&A, 155, 11

de Blok, W. J. G. 2010, AdAst, 2010, arXiv:0910.3538 [astro-ph.CO]

D'Onghia, E., Vogelsberger, M., & Hernquist, L. 2013, ApJ, 766, 34

Elmegreen, B. G., Seiden, P. E., & Elmegreen, D. M. 1989, ApJ, 343, 602

Fujimoto, M. 1966, AJ, 71, 856

Gittins, D. M., & Clarke, C. J. 2004, MNRAS, 349, 909

Goldreich, P., & Lynden-Bell, D. 1965, MNRAS, 130, 125

Gottesman, S. T., & Weliachew, L. 1975, ApJ, 195, 23

Hernquist, L. 1990, ApJ, 356, 359

Julian, W. H., & Toomre, A. 1966, ApJ, 146, 810

Kendall, S., Kennicutt, R. C., Clarke, C., & Thornley, M. D. 2008, MNRAS, 387, 1007

Kent, S. M. 1987, AJ, 93, 816

Lau, Y. Y. 1994, PhPl, 1, 2816

Lau, Y. Y., & Bertin, G. 1978, ApJ, 226, 508

Lin, C. C., & Lau, Y. Y. 1979, StAM, 60, 97

Lin, C. C., & Shu, F. H. 1964, ApJ, 140, 646

—. 1966, PNAS, 55, 229

Lisker, T., Grebel, E. K., & Binggeli, B. 2006, AJ, 132, 497

Lisker, T., Janz, J., Hensler, G., et al. 2009, ApJ, 706, L124

Lowe, S. A., Roberts, W. W., Yang, J., Bertin, G., & Lin, C. C. 1994, ApJ, 427, 184

Mark, J. W.-K. 1976a, ApJ, 203, 81

Mark, J. W. K. 1976b, ApJ, 205, 363

Mark, J. W.-K. 1977, ApJ, 212, 645

Masters, K. L., Mosleh, M., Romer, A. K., et al. 2010, MNRAS, 405, 783

Navarro, J. F., Frenk, C. S., & White, S. D. M. 1997, ApJ, 490, 493

Pannatoni, R. F., & Lau, Y. Y. 1979, PNAS, 76, 4

Patsis, P. A., Hiotelis, N., Contopoulos, G., & Grosbol, P. 1994, A&A, 286, 46

Roberts, W. W. 1969, ApJ, 158, 123

Roberts, Jr., W. W., Roberts, M. S., & Shu, F. H. 1975, ApJ, 196, 381

Roberts, Jr., W. W., & Shu, F. H. 1972, Astrophys. Lett., 12, 49

Rots, A. H. 1975, A&A, 45, 43

Sage, L. J., & Westpfahl, D. J. 1991, A&A, 242, 371

Sakhibov, F. K., & Smirnov, M. A. 1987, Soviet Ast., 31, 132

Sellwood, J. A. 2012, ApJ, 751, 44

—. 2013, in Planets, Stars and Stellar Systems. Volume 5: Galactic Structure and Stellar Populations, ed. T. D. Oswalt & G. Gilmore, 923

Shu, F. H., Milione, V., & Roberts, Jr., W. W. 1973, ApJ, 183, 819

Shu, F. H., Stachnik, R. V., & Yost, J. C. 1971, ApJ, 166, 465

Thomasson, M., & Donner, K. J. 1993, A&A, 272, 153

Toomre, A. 1963, ApJ, 138, 385

—. 1969, ApJ, 158, 899

Toomre, A. 1981, in Structure and Evolution of Normal Galaxies, ed. S. M. Fall & D. Lynden-Bell, 111

Toomre, A., & Kalnajs, A. J. 1991, in Dynamics of Disc Galaxies, ed. B. Sundelius, 341

Tremaine, S., & Weinberg, M. D. 1984, ApJ, 282, L5

Visser, H. C. D. 1980a, A&A, 88, 159

—. 1980b, A&A, 88, 149

Westpfahl, D. J. 1998, ApJS, 115, 203

Westpfahl, D. J., & Adler, D. S. 1996, in Astronomical Society of the Pacific Conference Series, Vol. 106, The Minnesota Lectures on Extragalactic Neutral Hydrogen, ed. E. D. Skillman, 96

Woodward, P. R. 1975, ApJ, 195, 61

Yun, M. S. 1992, PhD thesis, Harvard University, Cambridge, MA.

Yun, M. S., Ho, P. T. P., Brouillet, N., & Lo, K. Y. 1993, in Evolution of Galaxies and their Environment, ed. J. M. Shull & H. A. Thronson, 253

Yun, M. S., Ho, P. T. P., & Lo, K. Y. 1994, Nature, 372, 530

This preprint was prepared with the AAS LaTeX macros v5.2.

Table 1: Masses of three-component models

Mass ($\times 10^{10}$ $M_\odot$)	Lowe et al. (1994)	Kent (1987)	this work
disk	5.6	6.2	6.2
bulge	1.3 ($r < 12$ kpc)	1.0	1.5 ($r < 12$ kpc)
halo	3.0 ($r < 12$ kpc)	-	2.8 ($r < 12$ kpc)

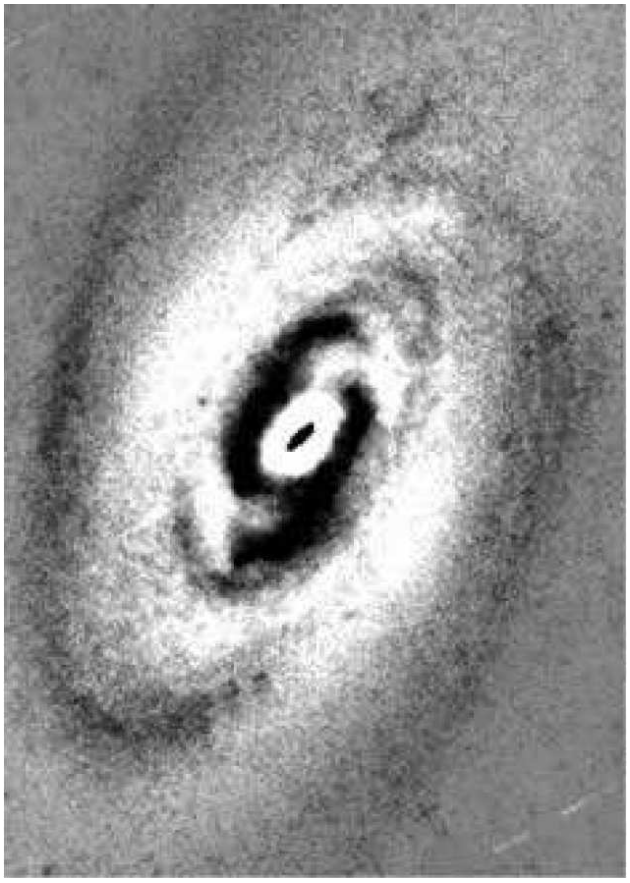

Fig. 1.— The non-axisymmetric residual for the IRAC 3.6 μm mass map (Kendall et al. 2008).

Table 2: Coefficients associated with the Toomre Q parameter

i	1	2	3
α_i	0.2	0.5	-0.1
β_i	0	0	10.0
γ_i	15.0	0.95	2.0

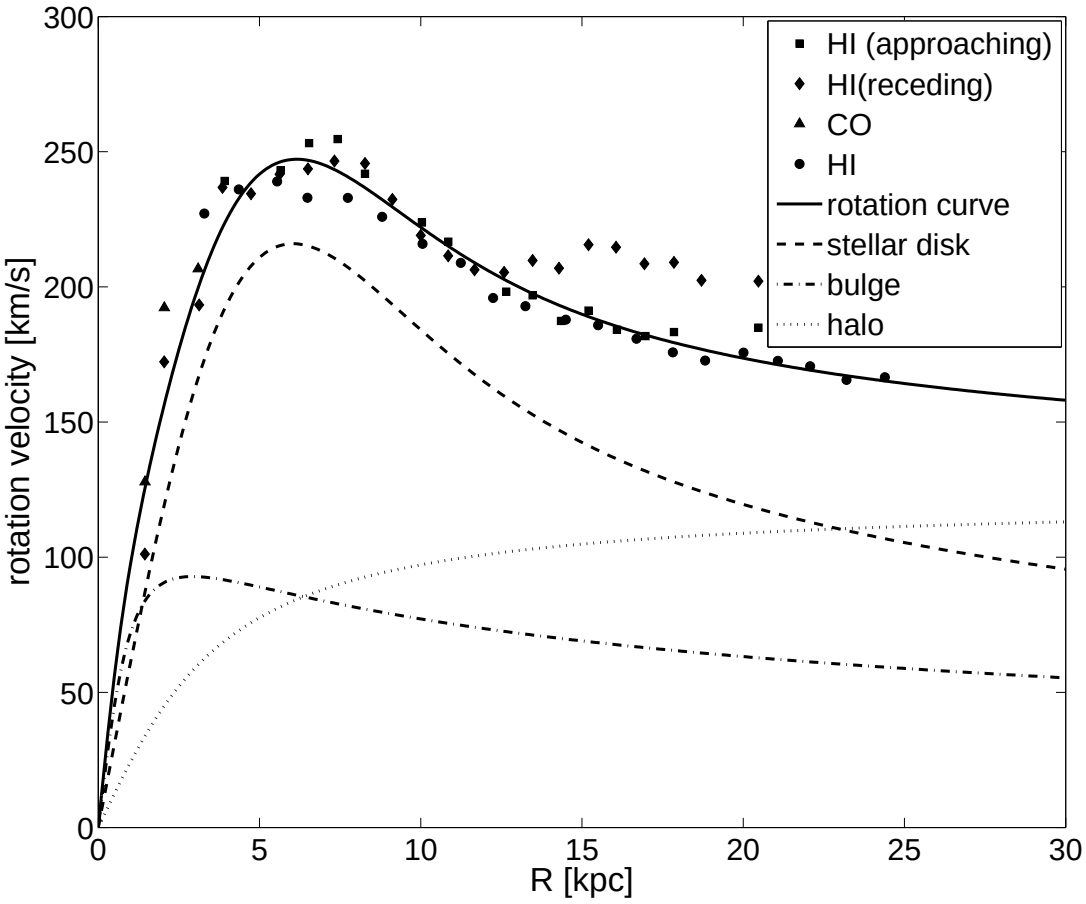

Fig. 2.— The rotation curve of M81. The filled circles are the HI data tabulated in Kent (1987). The diamonds and squares represent the HI observation on the receding and approaching sides, respectively (Adler & Westpfahl 1996). The CO data for the inner part of M81 are the triangles (Sage & Westpfahl 1991). The resultant rotation curve (solid line) resulting from contributions due to a stellar disk (dashed line), a bulge (dash-dotted line) and a dark matter halo (dotted line) is shown. The mathematical formulae used for these models are described in Sec. 2.1.

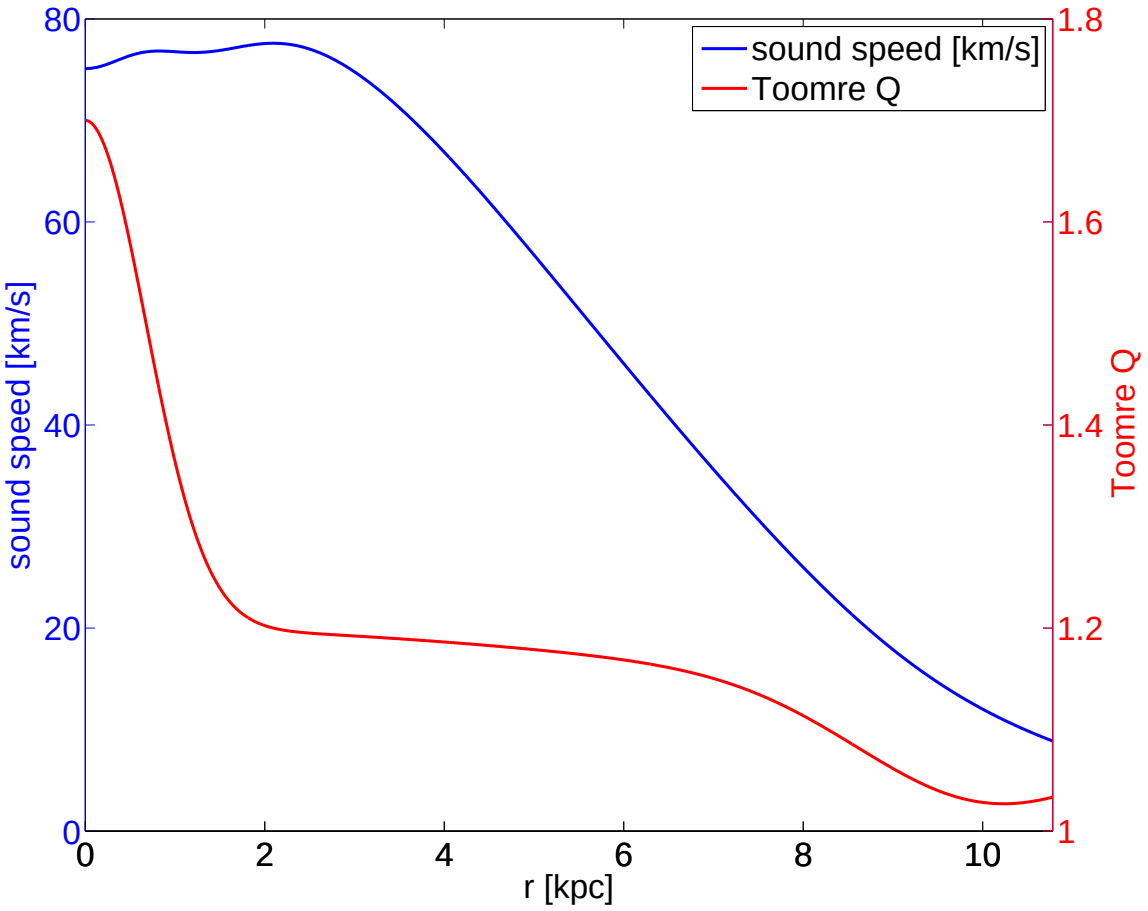

Fig. 3.— The Toomre's Q (right y-axis) parameter and the corresponding sound speed (left y-axis) as functions of galactocenter radius.

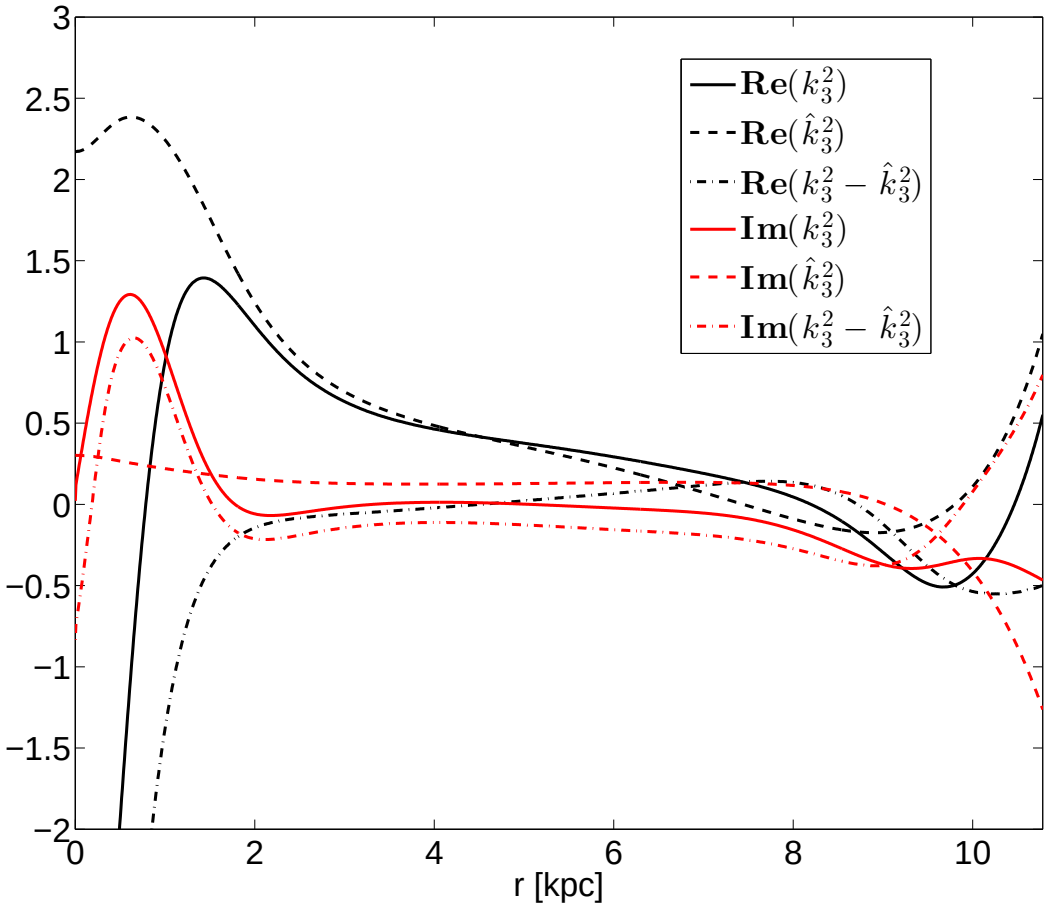

Fig. 4.— The real and imaginary parts of k_3^2, $\hat{k}_3^2$ and the sum of remaining terms.

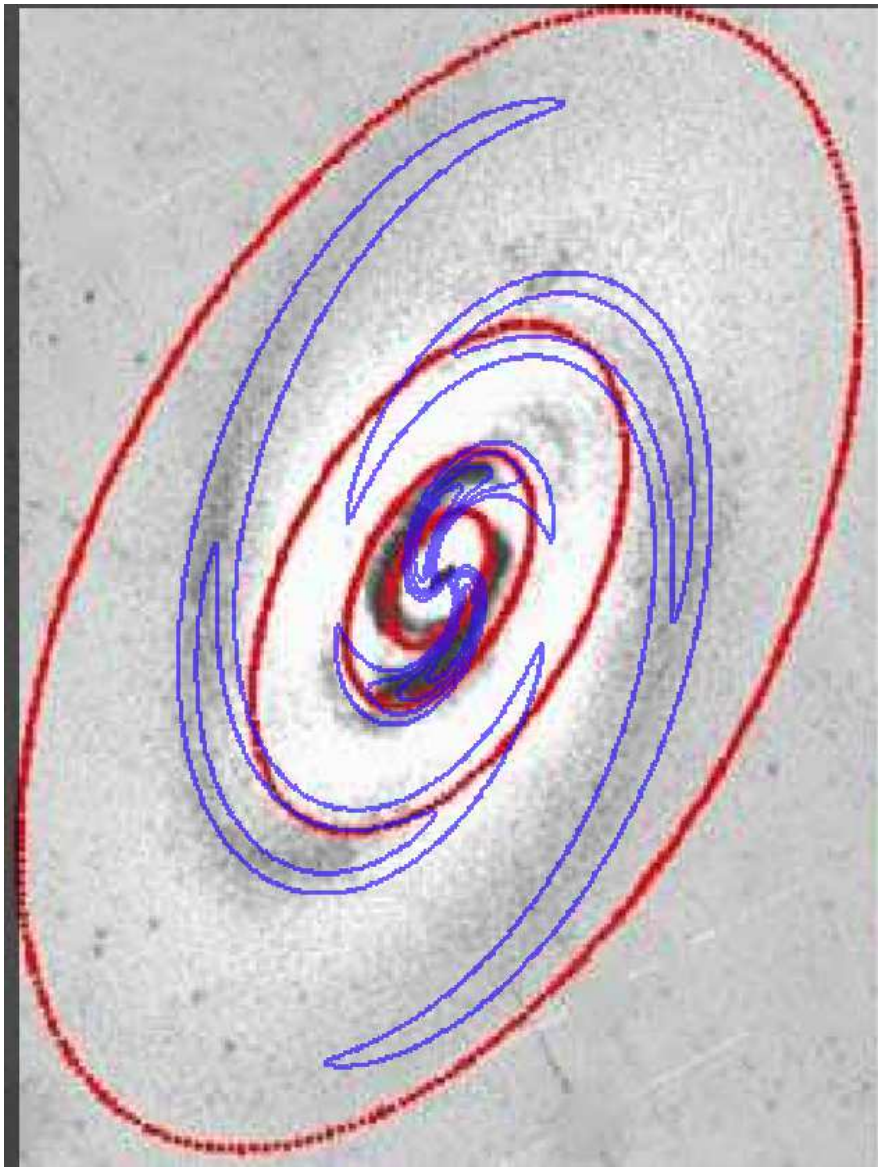

Fig. 5.— The contour map calculated from the mode analysis is overlapped on the residual map of IRAC 3.6 μm. The red ellipses, with increasing angular size, mark 80, 150, 300 and 675 arcsec, respectively.

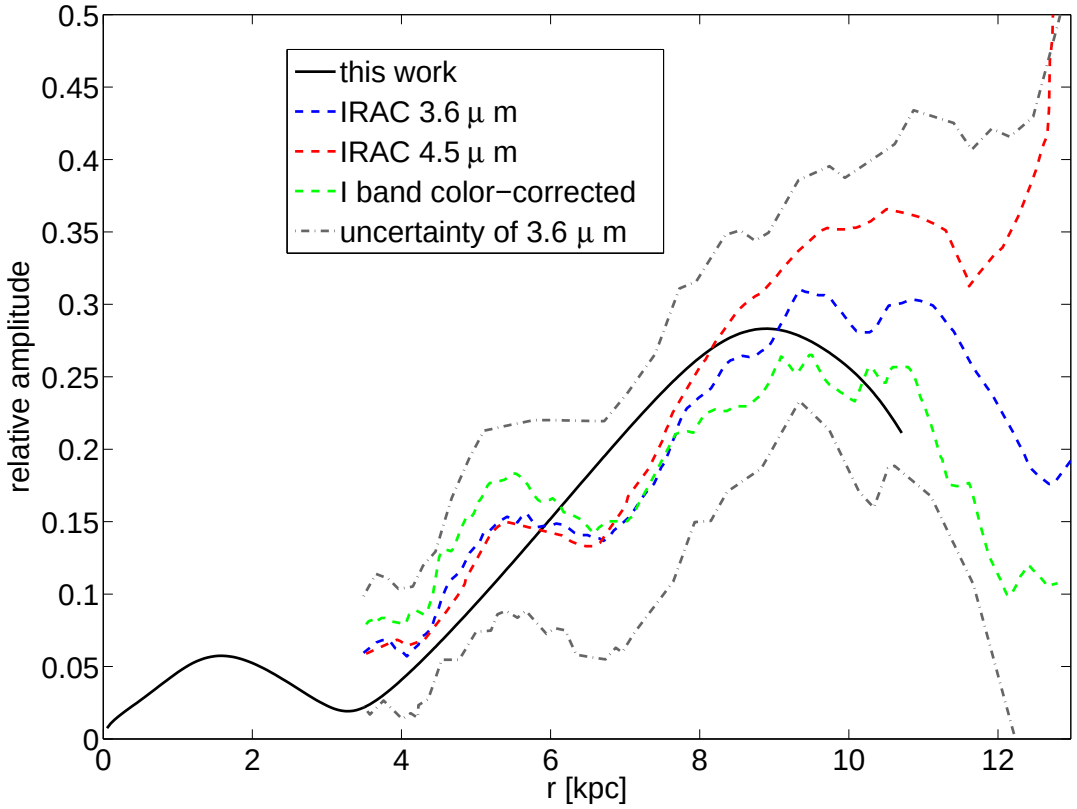

Fig. 6.— Relative amplitude of spiral density wave as a function of radius. The result obtained from linear theory of a spiral density wave is scaled to fit the observed data of different wavelengths. Within the range of uncertainty (bracketed by the grey dash-dotted curves), the general trend of the calculated waves (solid curve) is in good agreement with that of the observed data. The amplitude ripples seen in the observed curves are likely due to the interference of trailing waves and leading waves. This interference pattern has been implicitly neglected in this work due to the use of a radiation outer boundary condition.